CHEMISTRY OF MATERIALS

COMMUNICATION

pubs.acs.org/cm

Emergence of Room-Temperature Magnetic Ordering in Artificially Fabricated Ordered-Double-Perovskite Sr_2FeRuO_6

Jaewan Chang,[†] Kyujoon Lee,[‡] Myung Hwa Jung,[‡] Ji-Hwan Kwon,[§] Miyoung Kim,[§] and Sang-Koog Kim[†,*]

[†]National Creative Research Center for Spin Dynamics & Spin-Wave Devices and Nanospinics Laboratory, Research Institute of Advanced Materials, Department of Materials Science and Engineering, Seoul National University, Seoul 151-744, Republic of Korea

[‡]Department of Physics, Sogang University, Seoul 121-742, Republic of Korea

[§]Department of Materials Science and Engineering, Seoul National University, Seoul 151-744, Republic of Korea

KEYWORDS: artificial oxide superlattice, ordered double perivskite, Sr_2FeRuO_6, magnetism

Broken lattice symmetry at an oxide heterointerface, across which two different materials are bonded, is a source of exotic phenomena through modifications to existing physical interactions in isolated materials.[1] This possibility quite recently has been realized through vigorous research on (001)-oriented oxide heterostructures in which a maximum of two nearest-neighboring sites per transition metal ion can be modified and has illuminated the potential applications of oxides to future electronic devices.[2,3] Most of the magnetic or superconducting properties of (001)-oriented oxide heterostructures reported so far manifest themselves far below room temperature[4−8] and thus are not promising for their practical applications to devices operating at room temperature or higher. On the contrary, (111)-oriented oxide heterostructures have rarely been investigated, despite their possibility of more significant manipulation of electronic or magnetic interactions, for example, possibly inducing room-temperature physical properties by engineering up to six nearest-neighboring sites per transition metal ion.

For example, Sr_2FeRuO_6 (SFRO) is known as a disordered double perovskite that exhibits spin-glass behavior below the freezing temperature of ~60 K.[9] The disorder of the distribution of Fe^{3+} and Ru^{5+} ions at octahedral sites due to the insufficient charge-valence difference between them[10] contributes to spin frustration.[11] Ordered double perovskite (ODP) SFRO has never been successfully fabricated so far, although it lends itself to one of the best model systems with which the effectiveness of the engineering of nearest-neighboring octahedral sites in (111)-oriented heterostructures can be examined. In this Communication, we broaden the scope of investigation to the less-explored regime of (111)-oriented heterostructures. We employed a novel superlattice growth of (111)-oriented oxide heterostructure in order to overcome the thermodynamic restriction represented by ion disorder at the octahedral cation sites in SFRO. The subsequently engineered SFRO samples were found to be of ODP (see Figure 1) and to exhibit a magnetic ordering temperature up to 390 K.

Figure 1 is a schematic drawing of the crystal structure of the ODP-SFRO. All of the six nearest-neighboring sites of Fe^{3+} are occupied only by Ru^{5+} ions, and vice versa. Thus, there is only one kind of transition metal ion, either Fe^{3+} or Ru^{5+}, on each (111) plane (see Figure 1b), and Ru and Fe ions' (111) planes alternate in the [111] direction. Toward targeting the first

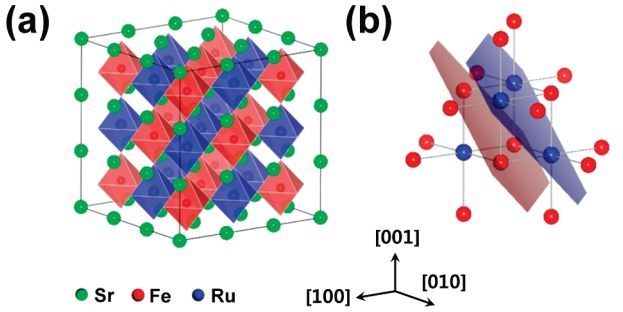

Figure 1. (a) Schematic illustration of alternating FeO_6 and RuO_6 octahedra (rock-salt-type ordering) in ODP-SFRO. The O^{2-} ions are omitted. (b) Nearest-neighbor representation of Ru and Fe ions in ODP-SFRO. The Sr^{2+} and O^{2-} ions are omitted for a clearer representation of the Ru and Fe octahedral ions' (111) atomic planes. The green, red, and blue spheres and the red and blue octahedra represent Sr, Fe, and Ru and FeO_6 and RuO_6, respectively.

fabrication of ODP-SFRO thin films, we employed an artificial superlattice-growth approach, using pulsed laser deposition (PLD), that is, alternate stacking of unit-cell-thick layers of [$SrRuO_3$ (SRO)] and [$SrFeO_3$ (SFO)] up to more than 55 periods on atomically flat Ti^{4+}-terminated $SrTiO_3$ (STO) (111) substrates. The details on the surface treatment of STO (111), which realizes an atomically flat single-terminated surface by virtue of thermal annealing combined with chemical etching, were provided in our previous work.[12] To effect stoichiometric ablations, sintered targets were impinged on using a KrF excimer laser (wavelength λ = 248 nm) of 2.0 J/cm^2 fluence with a spot area of 2.2 mm^2 and a laser repetition frequency of 4 Hz. The delay time between the SFO and SRO unit layers was 11−20 s. The oxygen pressure and substrate temperature were maintained at 100 mTorr and 700 °C, respectively. Prior to the superlattice deposition, around six-unit-cell-thick SRO buffer layers were deposited on the STO (111) substrates. The single steps and atomically flat terraces observed on the SRO buffer surfaces were nearly exact replicas of those observed on the STO (111)

Received: February 14, 2011
Revised: April 22, 2011
Published: May 05, 2011

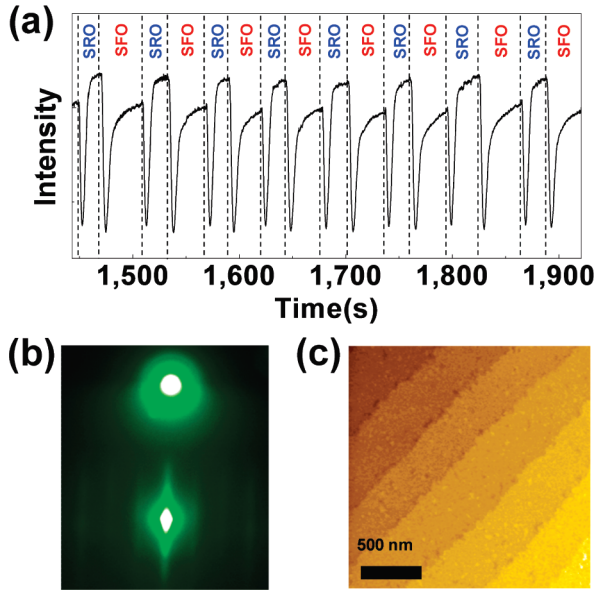

Figure 2. (a) Temporal variation of RHEED intensity recorded during growth of superlattice of $(SRO)_1(SFO)_1$. (b) RHEED pattern of the as-grown superlattice and (c) AFM surface morphology image ($2 \times 2\ \mu m^2$).

substrates, providing an ideal template indispensable for the layer-by-layer growth of the $(SRO)_1(SFO)_1$ superlattice.[13] In situ high-pressure reflection high-energy electron diffraction (RHEED) was employed for reliable digital control of the commensurate SRO and SFO layers during the film growth.[13,14] A 20 keV electron beam with an incidence angle of around 1.3° was used to record RHEED diffraction patterns and intensity profiles in specular reflection geometry.

As growth proceeded in the layer-by-layer mode, the two constituent materials exhibited their own characteristic and pronounced oscillation patterns, as evident in the RHEED profiles [see Figure 2a], which persisted until completion of the deposition. Figure 2b shows two-dimensional streaks in the corresponding RHEED pattern of the ODP-SFRO film, demonstrating its atomically flat surface. An atomic force microscopy (AFM) surface topographic image (Figure 2c) shows that the film surface consists of single steps and atomically flat terraces, nearly exact replicas of those on the STO (111) substrates, confirming the layer-by-layer growth mode of the films. The out-of-plane crystallographic information was obtained from $\theta-2\theta$ scan X-ray diffraction (XRD) patterns. Observation of the (222) and (444) reflection peaks evidence that the phase-pure films were grown epitaxially in the same out-of-plane orientation as that of the substrate. Furthermore, the presence of the (111) and (333) reflection peaks confirm the growth of a superlattice (Figure 3a), indicating well-defined interfaces between the SRO and SFO unit layers and, thus, a high degree of Fe^{3+}/Ru^{5+} ordering at the octahedral cation sites. The intensity ratio of the superlattice to the fundamental peak I_{111}/I_{444} is 0.072. On the basis of this ratio, the structural factors of the (111) and (444) reflections and the corresponding reflection angles, the ordering parameter S, which is defined as $S = 2(P_{Fe} - 0.5)$ with P_{Fe} the real occupancy of Fe at the Fe site of ordered double perovskite, was roughly estimated to be 0.5. Additionally, the in-plane crystalline information of the superlattice film was analyzed by XRD φ-scanning. The three-fold symmetry of the (440) reflection (Figure 3b) revealed a

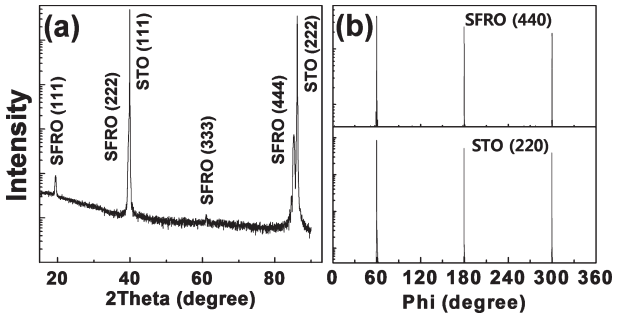

Figure 3. (a) $\theta-2\theta$ scan XRD. (b) φ-scan XRD of (440) reflections of ODP-SFRO (top) and (220) reflections of STO substrate (bottom).

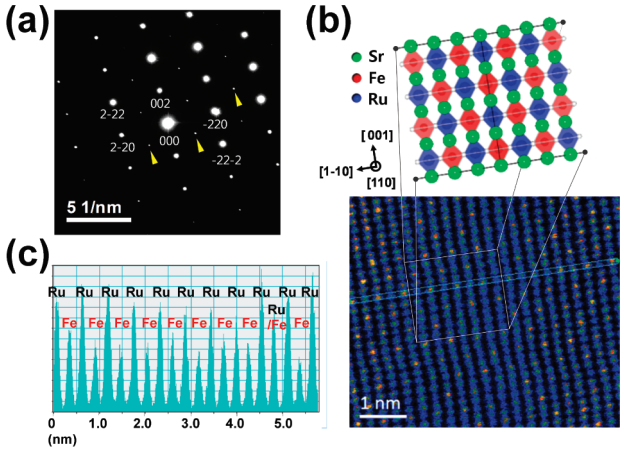

Figure 4. (a) [110] zone-axis TEM diffraction pattern of ODP-SFRO film. Some of the superlattice reflections are indicated by yellow arrows. (b) Top, (110) plane of ODP-SFRO; and bottom, cross-sectional Z-STEM image. (c) Intensity scan along the column indicated in the Z-STEM image shown in (b).

good in-plane orientation registry, reflecting the in-plane epitaxial relationship of $[1\bar{1}0]$ SFRO//$[1\bar{1}0]$ STO in pseudocubic representation.

The ordering of the Fe^{3+} and Ru^{5+} at the octahedral cation sites is more clearly revealed by the superlattice (lmn) (where l, m, and n are odd integers) reflections (evident as tiny spots), according to the transmission electron microscopy (TEM) diffraction pattern of an ODP-SFRO film (Figure 4a). Those reflections, resulting from the ordering of the Fe^{3+} and Ru^{5+} ions at the octahedral sites, were also visualized by [110] zone-axis Z-contrast scanning TEM (Z-STEM) (Figure 4b). As shown on the schematic projected (110) plane in the top of Figure 4b, the Fe^{3+} and Ru^{5+} ions are arranged in columnar, alternate order in the $[1\bar{1}0]$ direction, which arrangement is repeated in every other column in the [001] direction. An intensity scan in the column ($[1\bar{1}0]$ direction) (Figure 4c) reveals that there is a high degree of Fe^{3+}/Ru^{5+} ordering at the octahedral cation sites. These structural characterizations and analyses conclude that the grown suplattice films are ODP-SFRO, although their ordering at octahedral sites deviates from the perfect ordering, as revealed by the X-ray diffraction measurements. The deviation can be attributed to ion interdiffusion during the superlattice fabrication, in conjunction with the natural tendency of disordering of SFRO.

dx.doi.org/10.1021/cm200454z |*Chem. Mater.* 2011, 23, 2693–2696

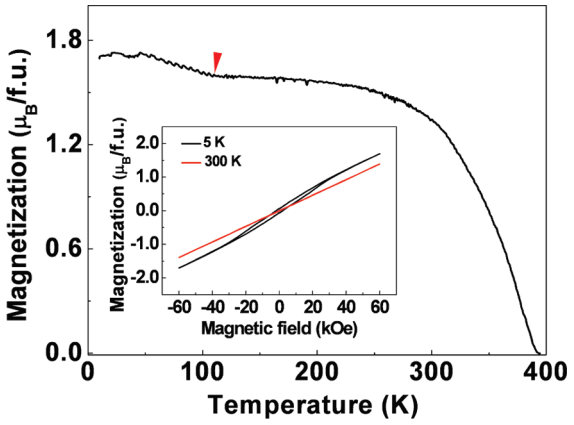

Figure 5. Temperature-dependent magnetization of an ODP-SFRO sample. An in-plane external magnetic field of 70 kOe was applied. The arrow indicates the starting point of the hump originating from magnetizations of the SRO buffer layer. Inset: field-dependent in-plane magnetization measured at 5 K (black line) and 300 K (red line).

Next, temperature-dependent magnetizations were measured using a superconducting quantum interference device-vibrating sample magnetometer. In preparation of the magnetization measurements, the as-grown films were postannealed in an oxygen atmosphere. The magnetic contribution of the STO substrate to the overall measured one was subtracted by following the same procedure with a bare STO (111) substrate. Figure 5 shows the temperature-dependent in-plane magnetization of the annealed ODP-SFRO sample, which has a magnetic ordering temperature up to $T_C \sim 390$ K. This is quite surprising, in that neither of the two constituent compounds exhibits ferromagnetism with such a high T_C: SRO is ferromagnetic below ~160 K[15] and SFO is antiferromagnetic below ~134 K.[16] Furthermore, bulk Sr_2FeRuO_6 exhibits only spin-glass behaviors with the freezing temperature of ~60 K.[11] The occurrence of the ferromagnetism (or ferrimagnetism) may be ascribed to the ordering of octahedral cations achieved by the engineering of nearest-neighboring sites. The ferromagnetism of ODP oxides (3d−4d or 3d−5d at octahedral cation sites) originates from spin-dependent band broadening and electron transfer attendant on the spin-dependent band shift, which result from spin-dependent hybridizations between t_{2g} states of 3d and 4d (5d) elements.[17] The magnetic moment of the 4d or 5d ions, then, is antiparallel to that of the 3d ion. Moreover, the greater proximity of Ru to ferromagnetism, as compared with Mo (4d) or Re (5d) in Sr_2FeMoO_6 and Sr_2FeReO_6, can contribute to the stabilization of the ferromagnetic state.[18] Given the expected spin-only value of 2 μ_B for antiparallel magnetic coupling of Fe^{3+} ($S = 5/2$) and Ru^{5+} ($S = 3/2$) ions, the observed magnetization of ~1.6 μ_B/f.u. at 70 kOe seems plausible, even though the value is lower than 2 μ_B, presumably due to antisite disorder.[19] The hump existing below ~115 K (indicated by the arrow in Figure 5) is attributable to the $SrRuO_3$ buffer that was deposited intentionally for the persistent layer-by-layer growth of the unit period of $(SRO)_1$-$(SFO)_1$. The height of the hump ($\sim 5 \times 10^{-6}$ emu) was ~1.05 μ_B/Ru, which is comparable to the magnetizations (0.42−1.4 μ_B/Ru) as obtained from ultrathin (001) SRO films.[20−22] The starting point of the hump (~115 K) is also close to the Curie temperature of ultrathin (001) SRO films (~110−130 K).[20,21] In-plane magnetization versus magnetic field data (inset of Figure 5) measured at 5 and 300 K show unsaturated magnetization even at 60 kOe, which can be attributed to the incomplete ordering at the octahedral sites with an ordering parameter of S = ~0.5. Disordered SFRO is known as a spin glass, exhibiting such unsaturated magnetization. The ODP-SFRO sample, however, did not exhibit the time-dependent magnetization relaxation, characteristic of spin glass, and clearly showed ferrimagnetic (or ferromagnetic) transition at ~390 K. The ODP-SFRO appeared to exhibit an intermediate behavior between an ideal ordered magnetic state and spin glass.

To summarize, we realized a fabrication of ODP-SFRO by growing superlattices of SRO and SFO layers, each of which has far-below-room-temperature magnetic orderings. ODP-SFRO samples exhibit a much enhanced magnetic transition temperature up to ~390 K. This work not only offers the first demonstration of ODP-SFRO fabrication but paves the way for possible fabrications of (111)-oriented oxide heterostructures of room-temperature intrinsic properties.

AUTHOR INFORMATION

Corresponding Author

*E-mail: sangkoog@snu.ac.kr.

ACKNOWLEDGMENT

The authors thank K.H. Kim and C.U. Jung for the valuable discussions. This work was supported by a grant (no. 2010-0000706) from the Basic Science Research Program through the National Research Foundation of Korea (NRF), funded by the Ministry of Education, Science and Technology. K.L. and M.H.J. acknowledge the support of the IT R&D program of MKE/KEIT (2009-F-004-01) and Sogang University's research grant (no. 201011014.01.). J.-H.K. and M.K. acknowledge an NRF grant (no. 20100017359).

REFERENCES

(1) Santamaria, J. *Nat. Phys.* **2006**, *2*, 229–230.
(2) Dagotta, E. *Science* **2007**, *318*, 1076–1077.
(3) Mannhart, J.; Schlom, D. G. *Science* **2010**, *327*, 1607–1611.
(4) Yu, P.; Lee, J.-S.; Okamoto, S.; Rossell, M. D.; Huijben, M.; Yang, C.-H.; He, Q.; Zhang, J. X.; Yang, S. Y.; Lee, M. J.; Ramasse, Q. M.; Erni, R.; Chu, Y.-H.; Arena, D. A.; Kao, C.-C.; Martin, L. W.; Ramesh, R. *Phys. Rev. Lett.* **2010**, *105*, 027201.
(5) Kozuka, Y.; Kim, M.; Bell, C.; Kim, B. G.; Hikita, Y.; Hwang, H. Y. *Nature* **2009**, *462*, 487–490.
(6) Reyren, N.; Thiel, S.; Caviglia, A. D.; Fitting Kourkoutis, L.; Hammerl, G.; Richter, C.; Schneider, C. W.; Kopp, T.; Rüetschi, A.-S.; Jaccard, D.; Gabay, M.; Muller, D. A.; Triscone, J.-M.; Mannhart, J. *Science* **2007**, *317*, 1196–1199.
(7) Brinkman, A.; Huijben, M.; van Zalk, M.; Huijben, J.; Zeitler, U.; Maan, J. C.; van der Wiel, W. G.; Rijnders, G.; A. Blank, D. H.; Hilgenkamp, H. *Nat. Mater.* **2007**, *6*, 493–496.
(8) Chakhalian, J.; Freeland, J. W.; Srajer, G.; Strempfer, J.; Khaliullin, G.; Cezar, J. C.; Charlton, T.; Dalgliesh, R.; Bernhard, C.; Cristiani, G.; Habermeier, H.-U.; Keimer, B. *Nat. Phys.* **2006**, *2*, 244–248.
(9) Battle, P. D.; Gibb, T. C.; Jones, C. W.; Studer, F. *J. Solid State Chem.* **1989**, *78*, 281–293.
(10) Anderson, M. T.; Greenwood, K. B.; Taylor, G. A.; Poeppelmerier, K. R. *Prog. Solid State Chem.* **1993**, *22*, 197–233.
(11) Gibb, T. C. *J. Mater. Chem.* **2005**, *15*, 4015–4019.
(12) Chang, J.; Park, Y.-S.; Kim, S.-K. *Appl. Phys. Lett.* **2008**, *92*, 152910–152912.
(13) Chang, J.; Lee, J.-W.; Kim, S.-K. *J. Cryst. Growth* **2010**, *312*, 621–623.

(14) Chang, J.; Park, Y.-S.; Lee, J.-W.; Kim, S.-K. *J. Cryst. Growth* **2009**, *311*, 3771–3774.
(15) Callaghan, A.; Moeller, C. W.; Ward, R. *Inorg. Chem.* **1966**, *5*, 1572–1576.
(16) Takeda, T.; Yamaguchi, Y.; Watanabe, H. *J. Phys. Soc. Jpn.* **1972**, *33*, 967–969.
(17) Fang, Z.; Terakura, K.; Kanamori, J. *Phys. Rev. B* **2001**, *63*, 1 80407(R).
(18) He, T.; Carva, R. J. *J. Phys.: Condens. Matter* **2001**, *13*, 8347–8361.
(19) Ogale, A. S.; Ogale, S. B.; Ramesh, R.; Venkatesan, T. *Appl. Phys. Lett.* **1999**, *75*, 537–539.
(20) Chang, Y. J.; Kim, C. H.; Phark, S.-H.; Kim, Y. S.; Yu, J.; Noh, T. W. *Phys. Rev. Lett.* **2009**, *103*, 057201.
(21) Xia, J.; Siemons, W.; Koster, G.; Beasley, M. R.; Kapitulnik, A. *Phys. Rev. B* **2009**, *79*, 140407(R).
(22) Izumi, M.; Nakazawa, K.; Bando, Y.; Yoneda, Y.; Terauchi, H. *Solid State Ionics* **1998**, *108*, 227–233.